Liquid redistribution in sheared wet granular media

Sudeshna Roy,* Stefan Luding,† and Thomas Weinhart‡
Multiscale Mechanics Group, Faculty of Engineering Technology, MESA+, University of Twente, P.O. Box 217, 7500 AE Enschede, Netherlands

(Received 1 August 2018; published 19 November 2018)

Shearing wet granular systems causes a redistribution of the interstitial liquid, which can affect the material's bulk behavior. Using the discrete-element method, we study the early rapid transients, the intermediate states, and the slow long-term evolution of liquid redistribution for various material parameters and different initial wetting conditions in an inhomogeneous split-bottom ring-shear cell featuring a wide shear band away from the system walls. In our model, liquid exists in two states, either in liquid bridges between particles or in liquid films on the particle surfaces. Under deformations like shear, the liquid is redistributed due to the rupture of existing and formation of new liquid bridges. Since we assume the immediate redistribution limit as a new model parameter, a liquid bridge limit volume is imposed to avoid extensive clustering of liquid. Studying the effect of the local shear rate on the liquid redistribution, two distinct effects are observed: For small amounts of shear, i.e., small strain amplitude, the interstitial liquid is randomly redistributed locally, and for larger amounts of shear, liquid is transported away from the shear zone. The local redistribution quickly results in a characteristic probability distribution of liquid bridge volumes, independent of the initial wetting conditions, but the mean and the shape of the distribution are dependent on the limit volume. Although the shear-driven diffusion-like liquid transport is active from the beginning, it dominates the transport in the long term, when the liquid moves out of the shear band, making the shear band dry. Ongoing theoretical analysis suggests a competition of drift and diffusive mechanisms in a different set of coordinates that can explain all our observations by defining a local Péclet number that quantifies the relative strength of the two transport mechanisms.

DOI: 10.1103/PhysRevE.98.052906

I. INTRODUCTION

The microstructure of confined granular media is typically inhomogeneous, anisotropic, and disordered [1,2]. Under external loading, these systems exhibit a nonequilibrium jamming transition from a solidlike to a liquidlike state [3–5] when the applied shear stress or energy exceeds the shear resistance or interparticle energy and materials start to flow. The microstructure is disturbed and rearranged completely during this process. Thus, the internal structure of the granular medium changes continuously when subjected to shear. This internal structure is influenced by polydispersity, related structural features, and frictional properties of the granular particles, which thus play a crucial role in determining their flow dynamics [6–11]. For example, shear tests of both drained and undrained sand show a state transformation, depending on the initial packing density, before it reaches a critical state [12–14]. This state transformation corresponds to a local maximum in the evolution of the coordination number. In a typical consolidated-drained condition, the pore water can drain out of the soil easily, causing volumetric strains in the soil and reaching the same critical state irrespective of the initial configuration.

Wet granular media are collections of grains containing unsaturated interstitial fluid, with athermal interactions through cohesive capillary, repulsive elastic, and dissipative contact forces. These capillary interactions are dependent on intrinsic properties of the contact force model, namely, the maximum capillary force and the maximum interaction distance [15]. External forces lead to granular flow if the applied shear stress exceeds the yield stress, eventually leading to a lower critical-state shear stress after finite shear strain [16–18]. A simple constitutive relation for the critical-state shear stress is constituted by the bulk cohesion and the macro friction coefficient [15,19,20]. The bulk cohesion is correlated with the Bond number or adhesion index, measured as the squared ratio of stress to wetting timescales [15,21]. This bulk cohesion was analyzed in terms of the force and fabric anisotropies [21] for wet granular materials. In our previous studies, a generalized rheology shows that the steady-state shear stress is factorized into a product of functions of different dimensionless numbers [18,22], if a simplistic situation is assumed where all contacts have an equal liquid bridge volume. The liquid in the system is then not treated as a separate entity; rather the contact model takes into account the effect of liquid capillary bridges.

Recent results by Mani *et al.* [23–25] show from experiments and simulations that the liquid content decreases within wet shear bands. This is a diffusion-driven phenomenon occurring at larger amount of shear, which causes the liquid to be transported away from the shear band. However, much remains unexplored of the initial redistribution of the liquid, which happens within a smaller shear strain scale and

*sudeshna84.roy@gmail.com
†s.luding@utwente.nl
‡t.weinhart@utwente.nl

is the major focus of our discussion. Within small shear strain, the liquid volume is conserved within the shear band, while the liquid is locally redistributed. This prompts us to look for a liquid migration model in our discrete element method (DEM) simulations where liquid moves between contacts due to shear-driven liquid bridge formation and rupture. Note that liquid transport fluxes are also driven by Laplace pressure changes [24,26–28], either through the vapor phase or through the wetting layers on the beads [29]. However, this mode of liquid transport is excluded from the discussion in this paper.

Understanding the role of shear on the redistribution of liquid in wet granular materials is of considerable technological importance for applications in many fields, such as civil engineering, pharmaceutical research, and agronomy, especially in process equipments subjected to inhomogeneous shear. One important application is the flow in industrial mixers and granulators. Note that the initial liquid distribution can vary significantly: The initial homogeneous liquid bridge volume in all contacts is observed if the initial wet sample is prepared by allowing equilibration by suction before shear. Conversely, another extreme situation is observed if all liquids are present in the form of liquid films and the initial sample is given a minimum equilibration time before shear [23]. We study here the transients of liquid redistribution upon shear, considering these two extremes of initial conditions. The question that comes to our mind is whether the liquid distribution reaches a steady or critical state which is independent of the initial configuration. In order to check this, we are investigating here the transient of liquid redistribution for wet granular media, after both small and large shear strains.

The paper is organized as follows. Section II describes the geometry of the system, details of the contact force models, the liquid migration model, and the different initial conditions for our simulations. Section III presents the methodology for the micro-macro transition in the transient states and for locating the shear band in the system. Sections IV A and IV B describe our results, giving an illustration of the small shear transients of liquid redistribution from different initial conditions towards an intermediate pseudocritical state of liquid distribution. Furthermore, we describe the effect of the different parameters, e.g., the width of the shear band, saturation, and the maximal liquid bridge volume on the transient evolution and the intermediate pseudocritical state in Secs. IV C, IV D, and IV E, respectively. Section IV F gives an overview of the state beyond the liquid redistribution transient when the liquid migrates out of the shear band by a shear-rate-dependent diffusive process on very large shears. We summarized and draw our conclusions in Sec. V.

II. SYSTEM

A. Geometry

The setup used for simulations consists of a shear cell with annular geometry and a split in the bottom plate, as explained in [15,17,18,22,30–34]. The system consists of an outer cylinder (radius $R_o = 110$ mm) rotating around a fixed inner cylinder (radius $R_i = 14.7$ mm) with a rotation frequency of $\Omega = 0.19$ s^{-1}. Note that we use a relatively fast rotation to save computational time. However, this is well below the dynamic flow limit. The granular material is confined by gravity between the two concentric cylinders and the bottom plate, with a free top surface. The bottom plate is split at radius $R_s = 85$ mm into a moving outer part and a static inner part. Due to the split at the bottom, a shear band is formed at the bottom at R_s. It moves inward and widens with increasing height, due to the geometry. This setup features a wide shear band away from the wall, free from boundary effects, if an intermediate filling height ($H \approx 40$ mm) is chosen. The focus of our study here is the liquid redistribution inside the system and the shear band in particular. While earlier simulations were done with an angular section of 90° [16,32–34] or 30° [15,18,22], very few simulations are done using the whole shear cell [35,36].

B. The DEM model

Our approach towards a microscopic understanding of macroscopic particulate material behavior is the modeling of particles using the so-called discrete-element method. We use the open source code MERCURYDPM [37,38] and in the following sections describe the particles and the contact model for our DEM simulations.

1. Particles

The annular space in the split bottom geometry mentioned above is filled with $N = 133\,892$ polydispersed spherical glass beads with density $\rho_p = 2000$ kg m^{-3} up to height $H \approx 40$ mm. The mean particle diameter is $r_\mathrm{p} = \langle r \rangle = 1.1$ mm and a homogeneous size distribution with $r_\mathrm{min}/r_\mathrm{max} = 1/2$ and width $1 - \langle r \rangle^2/\langle r^2 \rangle \approx 0.04$ is chosen.

2. Contact model for wet particles

We use a phenomenological contact model combining a linear viscoelastic repulsive force and a hysteretic nonlinear liquid bridge capillary force proposed by Willet *et al.* [39] based on the particle specifications, contact properties, liquid properties, and liquid saturation in the system [15]. The normal contact force between particles i and j is characterized by the linear elastic-repulsive and dissipative forces given by $f_n^{i,j} = k\delta - \gamma_0\dot{\delta}$ and the adhesive capillary force f_c^{ij} between particles i and j is given as

$$f_c^{ij} = \frac{f_c^{\max}\frac{r_\mathrm{eff}}{r_p}}{1 + 1.05\bar{S} + 2.5\bar{S}^2}, \tag{1}$$

where the separation distance is normalized as $\bar{S} = S\sqrt{r_p/V_b}$, $S = \max[0, |\vec{r}_i - \vec{r}_j| - (r_i + r_j)]$ being the separation distance between two particles i and j, with $\vec{r}_i$ and $\vec{r}_j$ the position vectors of the two particles, respectively. The maximum capillary force between the particles when they are in contact ($S = 0$) is given by $f_c^{\max} = 2\pi r_p \sigma \cos\theta$. The effective radius r_eff of the two interacting spherical particles can be estimated as the harmonic mean of the two particle radii r_i and r_j according to the Derjaguin approximation [40], yielding the effective radius

$$r_\mathrm{eff} = \frac{2r_i r_j}{r_i + r_j}. \tag{2}$$

TABLE I. Fixed parameters of the contact model.

Description	Quantity
surface tension σ	0.01 N m^{-1}
elastic stiffness k	120 N m^{-1}
contact angle θ	20°
sliding friction coefficient μ_p	0.01
viscous damping coefficient γ_0	5×10^{-3} kg s^{-1}

The adhesive force of the contact model is determined by three parameters: surface tension σ, contact angle θ of the liquid (both of which determine the maximum adhesive force), and the liquid bridge volume V_b (which determines how the force depends on the separation distance) [15]. The fixed parameters of the contact model are given in Table I. Bridges form when particles come into contact and rupture when the separation distance exceeds S_c. As proposed by Lian *et al.* [41], the critical separation distance S_c at which the bridge ruptures is given by

$$S_c = \left(1 + \frac{\theta}{2}\right) {V_b}^{1/3}. \tag{3}$$

C. Liquid migration model

In our present study we extend this model to account for liquid migration [15,18,22]. The methodology is quite straightforward as proposed by Mani *et al.* [23,25]: Liquid is transferred locally whenever contacts are formed or broken. The particles and the liquid are considered two different entities in the system. Liquid is associated either with a particle as a thin liquid film of volume V_f^i or with a contact as a liquid bridge of volume V_b^{ij}. We describe the liquid migration model in the following sections.

1. Liquid bridge formation

When two particles come into contact (i.e., overlap), a new liquid bridge is formed from the liquid contained in the particle films. Since there can be some liquid volume $V_{\min}$ trapped in the roughness of the grains [28,42], to contribute, V_f^i must be larger than or equal to $V_{\min}$. Therefore, the available liquid for bridge formation is $V_f^i - V_{\min}$. Since, $V_{\min}$ is fixed and trapped in the particles, without loss of generality, we assume $V_{\min} = 0$ for our simulations. The volume V_b^{ij} transferred to the liquid bridge is therefore

$$V_b^{ij} = \min\left(V_f^i + V_f^j, V_{\max}\right), \tag{4}$$

where $V_{\max} = \beta r_p^3$ is the maximal liquid bridge volume, imposed in our simulations as an additional parameter to avoid unbounded clustering of liquid by coalescence. This model is designed for small liquid content and large contact angle with fast and easy transport of fluid on the surface. Figure 1 shows a schematic of liquid bridge formation.

The excess volume $V_f^i + V_f^j - V_b^{ij}$ remains as film volume in the interacting particles, in proportion to the existing volume per particle. The appropriate value for $V_{\max}$ can be estimated by different arguments. An upper bound for β is due to the maximal pore space available, which implies for

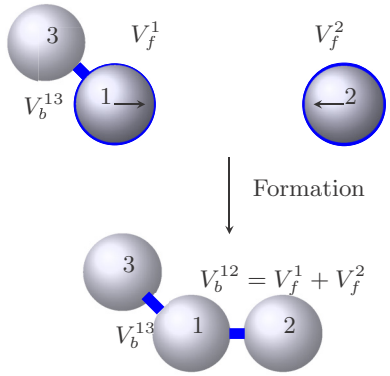

FIG. 1. Liquid bridge formation ($V_b^{12} < V_{\max}$).

random close packing of monodisperse spheres that $\beta \approx 0.33$, if all pore space would be filled by liquid. However, we rather assume poor saturation and localization of liquid at the contacts and thus consider, following the arguments from [42], that $\beta = 0.058$. Thus, liquid bridges remain in the pendular limit, filling less than 20% of the pore space [43]. Beyond the pendular regime, a considerably more complex expression for the liquid bridge force is given for greater volumes and contact angles [39], however, the difference from our simple expression is below 20% even for much larger β, so we refrain from using a too complex expression and stick to Eq. (1). The local adhesive force, as quantified by the Bond number Bo, does not change with liquid volume for either capillary force model and only a few liquid bridges are assumed to grow really large. Nevertheless, we explore below the effect of the maximum volume $V_{\max}$ on the liquid redistribution, using different β in the range

$$\beta \in [0.03, 0.08, 0.15, 0.23, 0.45, 0.60]. \tag{5}$$

2. Liquid bridge rupture

When the distance between two particles i and j with a liquid bridge in between exceeds the rupture distance of the liquid bridge, the liquid bridge ruptures and the bridge volume is distributed to the neighboring contacts

$$V_b^{mn,\text{new}} = \min\left(V_b^{mn,\text{old}} + V_b^{ij}/2N_c^m, V^{\max}\right), \tag{6}$$

where n denotes the particles in contact with one of the two particles $m \in i, j$ and N_c^m is the number of neighboring contacts associated with the particle m. Figure 2 shows a schematic representation of liquid bridge rupture. If the maximum volume $V_{\max}$ is reached, the remaining liquid is added to the film volumes V_f^i and V_f^j. Thus, total liquid volume conservation is ensured.

D. Initial conditions

We begin our simulations with a no-shear preparation history, where we allow particles to fall freely into the system under gravity. At this stage, particles are dry without any liquid on them. After free falling, the particles are allowed to relax until they reach a ratio of kinetic to potential energy below 10^{-3}. After relaxation, the kinetic energy of the system becomes negligible while there is a finite elastic potential

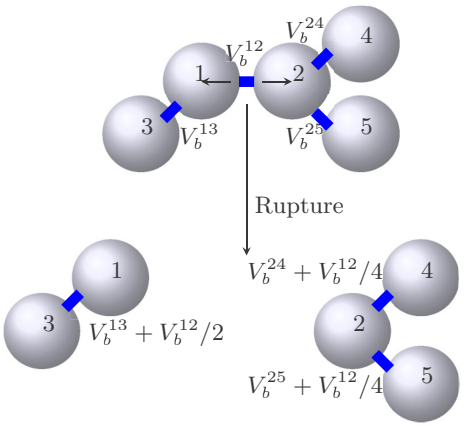

FIG. 2. Liquid bridge rupture ($V_b^{ij,\text{new}} < V_{\max}$, where $i \in 1, 2$ and $j \in 3, 4, 5$).

energy, which contributes to the total energy of the sample. After the complete preparation and relaxation of the sample, we add liquids to the system and start shearing. The potential energy of the sample is increasing after addition of the liquid, depending on the saturation, while the kinetic energy remains small at the commencement of shear.

Liquid addition means that each particle is assigned with an initial liquid film volume V_f^0. If not specified otherwise, we have $V_f^0 = 50$ nl in our system for standard simulations discussed in this paper. On shearing, the kinetic energy increases and the elastic potential energy changes slowly until they reach a steady state with $E_k/E_p \approx 10^{-6}$. In order to understand how liquid redistributes, we simulate the two extreme cases of initial liquid distribution: (i) 100% liquid distribution in the form of liquid films (initial condition A) and (ii) 100% liquid distribution in the form of liquid bridges (initial condition B). Initial condition A is initialized by distributing the total amount of liquid volume uniformly among all the particles as liquid film at the start of the simulation. This amounts to $V_f^0 = 50$ nl liquid film volume per particle. However, few liquid bridges are already formed in the detected contacts at the onset of shear. Initial condition B is done by distributing the same amount of liquid volume as in initial condition A, uniformly among all the existing contacts as liquid bridges. The contacts here include both the physical contacts and the possible long-distance interactions between particles that are within the range of rupture distance of the liquid bridge. It is obvious that when the wet sample is allowed with long equilibration time, even distant surfaces could be filled in with liquid bridges due to suction pressure gradient. Thus, it is a logical assumption to distribute the liquid into not only the mechanical contacts, but also the long-range contacts within the range of rupture distance.

Granular materials with interstitial liquid can be classified as dry bulk, adsorption layers, pendular state, funicular state, capillary state, or suspension, depending on the level of saturation [44,45]. In our present work we intend to study the phenomenology of liquid bridge redistribution between particles in the pendular state, where well-separated liquid bridges exist individually, without geometrical overlap. In order to study the influence of liquid content on the liquid redistribution, we vary the initial liquid film volume V_f^0 on the particles given as

$$V_f^0 \in [10, 20, 50, 80, 100] \text{ nl}, \tag{7}$$

corresponding to saturation [43]

$$S \in [2.99\%, 5.98\%, 14.95\%, 23.92\%, 29.90\%], \tag{8}$$

corresponding to a measured average porosity of 0.35. While varying V_f^0, we keep the maximal liquid bridge volume constant with $V_{\max} = 40$ nl ($\beta = 0.03$). While varying β according to Eq. (5), we keep the initial liquid film volume constant with $V_f^0 = 50$ nl. As a standard simulation in this paper, we keep the initial liquid film volume $V_f^0 = 50$ nl and the maximal liquid bridge volume constant with $\beta = 0.03$, if not specified otherwise. The bulk saturation is 14.95% for this standard case, with a bulk porosity of $\epsilon \approx 0.35$ measured from the simulations.

III. MICRO-MACRO TRANSITION

To extract macroscopic properties from the DEM, we use the spatial coarse-graining approach. This technique was used earlier in Refs. [16,33,34]. The averaging is performed over toroidal volumes, assuming rotational invariance in the tangential direction over several snapshots of time. The averaging procedure for a three-dimensional system is explained in [15,17]. The simulation is run for a total time of 22 s and transient data are obtained by temporal averaging over every five snapshots with steps of 0.015 s, starting from the onset of shear. We obtain the local macroscopic quantities such as shear rate $\dot{\gamma}$, liquid bridge volume V_b, liquid film volume V_f, and the contact number C_w for further analysis. We distinguish between the contacts with liquid bridges and without, which is significant for wet granular materials.

A. Identifying the shear band

We analyze the evolution of the liquid bridge volumes for initial conditions A and B as explained in Sec. II D. The objective is to study the transients of liquid redistribution under shear. Thus, we focus on the region inside the shear band where dry systems reach a critical state after large enough shear. We define the shear band region by accumulating all local points having shear rate higher than a threshold value. This threshold value varies at every height and is defined as a fraction α of the maximum shear rate at the center of the shear band at a given height $\dot{\gamma}_{\max}(z)$. Thus, we consider the shear band region as all local points having shear rate $\dot{\gamma}(r, z) \geqslant \alpha\dot{\gamma}_{\max}(z)$ as shown in Fig. 3. For dry granular systems, the critical state is achieved at a constant pressure p and local shear rate condition over regions with shear rate larger than a certain α (dependent on the duration of shear) corresponding to the region of system that was sufficiently sheared to be restructured.

B. Wet shear band phenomenology

While the shear band is well established above this shear rate for wet granular materials also, our analysis in later sections shows that the liquid redistribution is averaged over

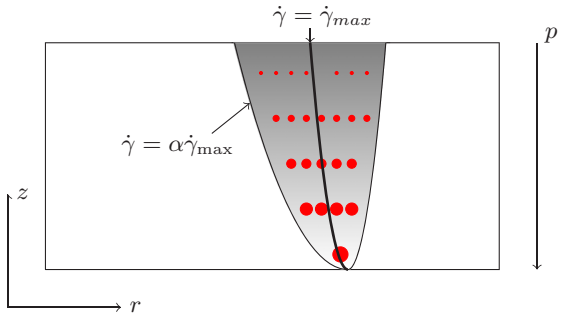

FIG. 3. Schematic diagram of simulation setup showing the shear band. Red dots indicate local points for our analysis with the size of the dots given by the local pressure. The gray shaded area denotes the shear band ($\dot{\gamma} > \alpha\dot{\gamma}_{\max}$) and the bold line shows the shear band center ($\dot{\gamma} = \dot{\gamma}_{\max}$).

the shear band region corresponding to $\alpha = 0.4$ at different heights in the system. Additionally, the relative shear rate threshold α is varied from 0 to 0.8 to inversely vary the width of the shear band to see its effect. Thereby, we extract local data (shown by the red dots) corresponding to the regions as marked by the shaded area in Fig. 3. We see the evolution of the macro quantities such as the mean liquid bridge volume $\langle V_b \rangle$ and the contact number C_w corresponding to the region inside the shear band as a function of local shear γ. We then analyze the transients for the shear band evolution to obtain the transients for liquid redistribution inside the shear band.

IV. RESULTS

The main objective of our work is to understand the liquid bridge volume redistribution process under shear. We show in Secs. IV A and IV B that different initial conditions of liquid bridge volume lead to the same redistribution of liquid bridge volumes when sheared to an intermediate state. This intermediate state, when the liquid bridge volume becomes independent of the initial conditions, is termed the pseudocritical state. Furthermore, we describe the effect of the different parameters, e.g., the width of the shear band, saturation, and the maximal liquid bridge volume, on the transient evolution and the intermediate pseudocritical state in Secs. IV C, IV D, and IV E, respectively. Section IV F gives an overview of the state beyond the liquid redistribution transient when the liquid migrates out of the shear band by a shear-rate-dependent diffusive process on very large shears.

A. Transients for liquid redistribution

In this section we describe the transients for liquid redistribution for unsaturated granular materials subjected to shear with different initial conditions for initial conditions A and B as explained earlier. For our analysis of the redistribution of the liquid bridges, we obtain the histogram distribution of the liquid bridge volume at different times with 100 bins of the histograms. We show the overlay of the histograms of liquid bridge volume distribution at different times with lines instead of the bars as shown in Fig. 4.

We obtain the global shear $\gamma_g = 2\pi R_o \Omega \Delta t/(R_o - R_i)$ by scaling the distance traversed by a particle on the outer wall

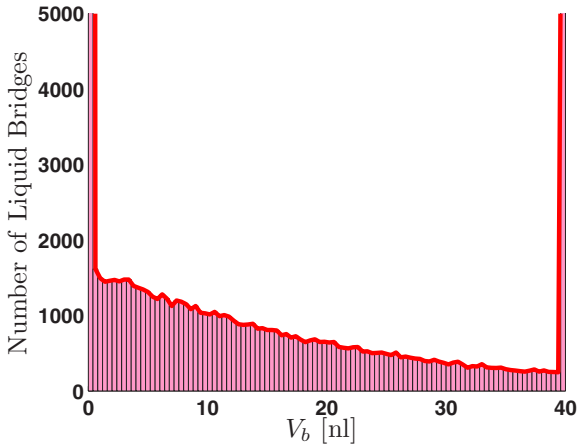

FIG. 4. Overlaying of the histogram of the liquid bridge volume distribution with lines for $\dot{\gamma}(r, z) \geqslant 0.4\dot{\gamma}_{\max}(z)$ after 6.03 s ($\gamma_g = 8.23$) for initial condition A.

$2\pi R_o \Omega \Delta t$ in time Δt by the distance between the annular space $R_o - R_i$. We use that scaling factor as this is very simple and dependent on the geometry of the system. There can be other length scales, such as the width of shear band, which is about half this geometry-dependent scale $R_o - R_i$, or the particle diameter $2r_p$, which is about 40 times smaller. Figure 5(a) shows the evolution of liquid bridge volume distribution over global shear γ_g for initial condition A. Initially, the mean distribution of liquid bridge volume is lower than the intermediate pseudocritical-state distribution of liquid bridge volume. We start from an initial condition of all particles having a liquid film of volume $V_f^0 = 50$ nl. Then liquid bridges are formed, even at no shear condition, wherever contacts are detected, in random sequence. Hence, the initial liquid bridge distribution number is lower than the intermediate pseudocritical state. The initial liquid volume distribution ($\gamma_g = 0$) shows spikes at volumes of 40, 30, 20, 10, and 0 nl. Those spikes are a numerical artifact of having a uniform initial liquid film volumes $V_f^0 = 50$ nl and setting a fixed maximum allowable liquid bridge volume of $V_{\max} = 40$ nl. Thus, those spikes are expected to vanish for slow redistribution of liquid bridges, for less homogeneous initial distributions, or by also not restricting the maximum allowable liquid bridge volume. The smaller liquid bridge volumes have a higher count than the larger liquid bridge volumes, but an accumulation in number of the maximal liquid bridge volumes ($V_b = V_{\max}$) is found. With increasing shear, liquid of the maximal bridges is redistributed to the smaller liquid bridges and the overall liquid volume is conserved inside the shear band in this small shear strain.

Figure 5(b) shows the liquid bridge volume redistribution over global shear for initial condition B. Initially, the distribution of liquid bridge volume is nonuniform, with a high count of the intermediate liquid bridge volumes between 10 and 20 nl (higher than the intermediate pseudocritical state), the initial liquid bridge volume being $V_b^0 \approx 11$ nl. Other liquid bridges have lower count (lower than the intermediate pseudocritical state) at the initial state. With increasing global shear, liquid from the intermediate volume of liquid bridges is redistributed to other liquid bridges and the overall liquid

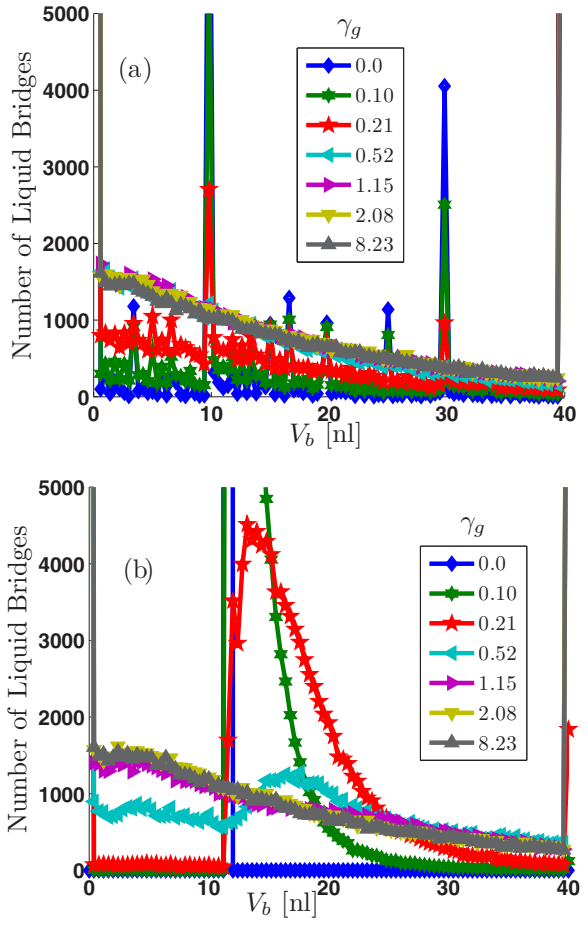

FIG. 5. Liquid bridge volume distribution for different initial conditions of (a) 100% liquid film (initial condition A) and (b) 100% liquid bridge (initial condition B) for $\dot{\gamma}(r,z) \geqslant 0.4\dot{\gamma}_{\max}(z)$.

volume is conserved inside the shear band in this small shear strain. Comparing Figs. 5(a) and 5(b), it is observed that initial condition A reaches the equilibrium state faster than initial condition B. Note that the local shear γ inside the shear band center and near the split position of the shear cell is of the same order and approximately 2 times the value of the global shear γ_g. Thus, the legends shown in Figs. 5(a) and 5(b) in terms of global shear are not the quantitative representation of the local shear inside the shear band. The evolutions of the two limits [that fall outside the range of Figs. 5(a) and 5(b)], the number of liquid bridges with $V_b = 0$ (given by the red and blue ○) and $V_b = V_{\max}$ (given by the red and blue ◇), are shown in Fig. 6. Irrespective of the different transients' behavior, both the number of dry contacts and the maximal liquid bridge contacts reach the same value given by the plateau in the intermediate pseudocritical state.

B. Liquid redistribution towards an intermediate pseudocritical state

Liquid redistribution in unsaturated granular media is associated with the formation of new liquid bridges and the rupture of existing liquid bridges. Figure 7 shows a comparison of the distribution of the liquid bridge volumes after 6.01 s for the two different initial conditions A and B. Evidently, an

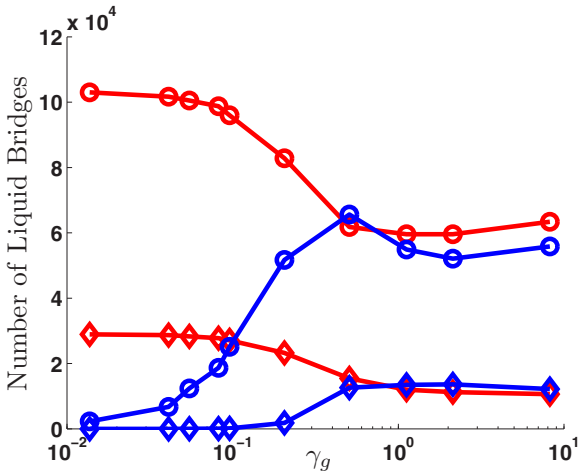

FIG. 6. Number of liquid bridges with $V_b = 0$ nl (dry contacts) for initial conditions A and B (red and blue ○, respectively) and number of liquid bridges of volume $V_b = V_{\max}$ for initial conditions A and B (red and blue ◇, respectively) as a function of global shear γ_g for $\dot{\gamma}(r,z) \geqslant 0.4\dot{\gamma}_{\max}(z)$.

intermediate state is reached where the rate of liquid bridge formation is balanced by the rate of liquid bridge rupture and is attained irrespective of the initial distribution of the liquid in the system. Here we focus at the whole shear band region $[\dot{\gamma}(r,z) > 0.4\dot{\gamma}_{\max}(z)]$ and confirm that the system reaches an intermediate state independent of the initial conditions. In Sec. IV C we focus on the liquid redistribution in the different regions of the shear band.

Figure 8(a) shows the mean liquid bridge volume per wet contact $\langle V_b \rangle$ as a function of local shear inside the shear band for initial conditions A and B. For each initial condition, the data points collapse onto a single curve. Figure 8(b) shows the wet contacts per particle C_w as a function of local strain for initial conditions A and B. Again, the data collapse for each initial condition. Thus, the change in mean liquid bridge

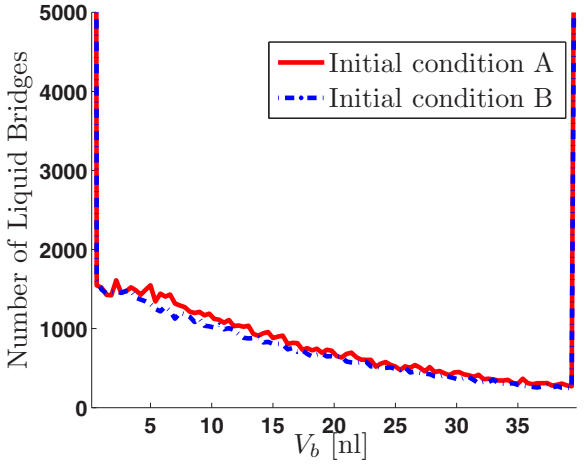

FIG. 7. Overlay of the liquid bridge volume distribution for initial condition A (red solid line) and initial condition B (blue dash-dotted line) for $\dot{\gamma}(r,z) \geqslant \alpha\dot{\gamma}_{\max}(z)$ and $\alpha = 0.4$ after 6.03 s ($\gamma_g = 8.23$).

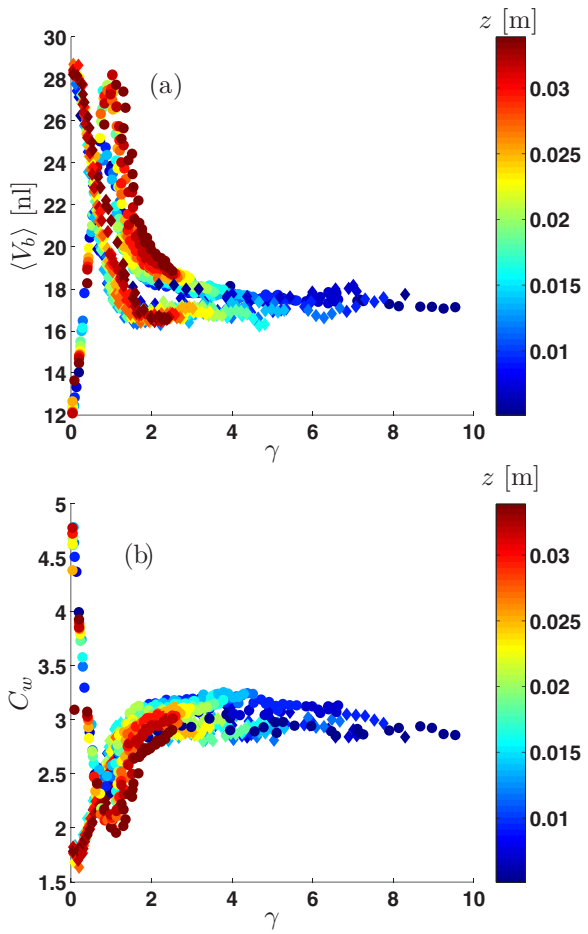

FIG. 8. (a) Mean liquid bridge volume per contact $\langle V_b \rangle$ as a function of local strain for initial condition A ($\diamond$) and initial condition B ($\circ$) and (b) wet contacts per particle C_w as a function of local strain for initial condition A ($\diamond$) and initial condition B ($\circ$) for $\beta = 0.03$ nl, for $\dot{\gamma}(r, z) \geqslant 0.4\dot{\gamma}_{\max}(z)$. Different colors indicate different heights.

volume per wet contact over shear observed inside the shear band center for initial conditions A and B is an intrinsic phenomenon undergone by each local point inside the shear band before they reach the intermediate pseudocritical state. Initial condition A shows a decrease in mean liquid bridge volume per contact with increasing shear. This can be related to Fig. 5(a) as the maximal liquid bridge volumes ($V_{\max}$) are distributed to a larger number of smaller bridges until they reach the intermediate pseudocritical value. Starting with an initial uniform liquid bridge volume distribution of $V_b^0 \approx 11$ nl, initial condition B shows an initial increase in mean liquid bridge volume per contact with increasing shear until it reaches a peak mean volume of liquid bridge approximately $V_b^{\mathrm{p}} \approx 28$ nl. Further, the mean liquid volume per contact decreases with increasing shear until they reach the intermediate pseudocritical state $V_b^{\mathrm{c}} \approx 17$ nl. Both initial conditions A and B reach the same intermediate state in terms of mean liquid bridge volume per wet contact. The number of wet contacts per particle shows an inverse functional behavior as $\langle V_b \rangle$, as the liquid saturation remains constant, but reaches the same intermediate state too for initial conditions A and B. The total elastic potential energy of the system also reaches the same state for the two initial conditions, irrespective of the different energy they have in the transients, which depends on the number of dry and wet contacts in the transients.

During the process of redistribution of liquid, the liquid volume is approximately conserved inside the shear band within the range of this small shear scale, when diffusion is less dominating. The liquid bridge volumes are redistributed during the process of contact breaking and formation. For initial condition A, as observed in Fig. 6, a significant number of liquid bridges have the maximal volume. Subsequently, more smaller liquid bridges are formed at the cost of rupture of these critical volume liquid bridges, resulting in an increase in the number of wet contacts per particle and a decrease in the mean liquid bridge volume per wet contact as shown in Figs. 8(a) and 8(b). For initial condition B, as observed from Figs. 5(b) and 6, the number of liquid bridges with higher liquid volume initially increases with time. In the initial state, all the contacts have an equal liquid bridge volume V_b^0. When subjected to shear, many contacts break, resulting in distributing the liquid to the neighboring contacts, making them grow in liquid bridge volume content. Hence, here the mean liquid bridge volume increases at the cost of breaking contacts. Simultaneously, the number of wet contacts C_w decreases as shown in Fig. 8(b). Thus, in this initial condition wet contacts are subjected to shear break or rupture more or less instantaneously, distributing the liquid to the neighboring existing contacts and resulting in a rapid increase in mean liquid bridge volume and a decrease in the number of wet contacts before equilibrating towards the pseudocritical state.

C. Dependence on the relative shear rate threshold

As explained in Sec. III A, we define the shear band region by accumulating all local points having shear rate higher than a threshold value. This threshold value varies at every height and is defined as a fraction α of the maximum shear rate at the center of the shear band at a given height $\dot{\gamma}_{\max}(z)$. Thus, we consider the shear band region as all local points having shear rate $\dot{\gamma}(r, z) \geqslant \alpha\dot{\gamma}_{\max}(z)$. It is evident that the span of the shear band region can be varied by varying α. A stable shear band is observed, with a steady pressure and shear rate, over regions with shear rate larger than the value $\alpha\dot{\gamma}_{\max}(z)$, $\alpha = 0.1$. The local shear rate $\dot{\gamma}$ is highest at the shear band center and drops as a Gaussian function of the distance from the center of the shear band at a given pressure [30,46]. We vary the width (or distance from the center) of the shear band by varying $\alpha =$ 0.0–0.8 and thereby see the effect on the liquid redistribution. Figure 9(a) shows the liquid distribution of wet contacts for different α, excluding the values for $V_b = 0$ and $V_b = V_{\max}$. Naturally, the number of contacts increases with decreasing α. However, while we observe a uniform difference between the number of contacts between $\alpha = 0.4$ and 0.8, a nonuniform difference is observed between $\alpha = 0.0$ and 0.4. Figure 9(b) shows the normalized liquid bridge distribution for different width of the shear band. Note that here we normalize the histogram for liquid bridge distribution by scaling with the total number of liquid bridges in the given histogram. The normalized distributions collapse for all widths of the shear band, signifying that the liquid bridge distribution is identical

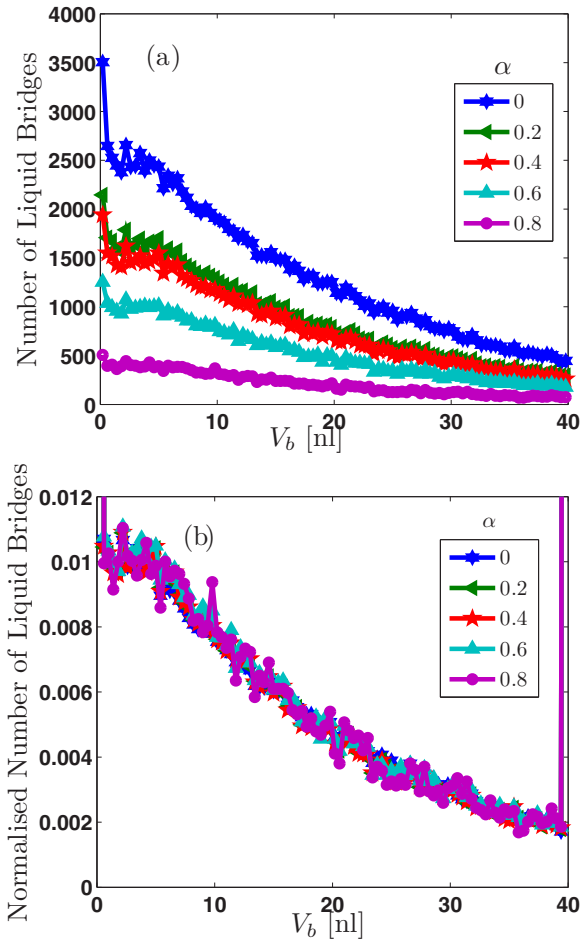

FIG. 9. (a) Liquid bridge volume distribution and (b) normalized liquid bridge volume distribution for initial condition B for $\dot{\gamma}(r,z) \geqslant \alpha\dot{\gamma}_{\max}(z)$ and α varied from 0 to 0.8 after 6.03 s ($\gamma_g = 8.23$).

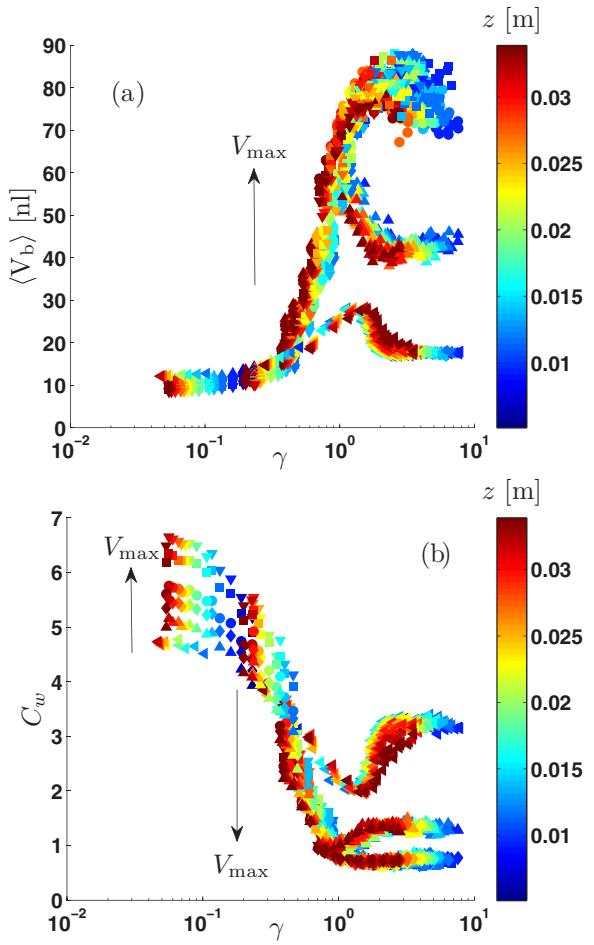

FIG. 10. (a) Mean liquid bridge volume per contact and (b) fraction of wet contact as a function of local strain for initial condition B for different maximal liquid bridge volume quantified by β, $\beta = 0.03$ ($\triangleleft$), $\beta = 0.08$ ($\triangle$), $\beta = 0.15$ ($\diamond$), $\beta = 0.23$ ($\circ$), $\beta = 0.45$ ($\square$), and $\beta = 0.60$ ($\triangledown$) for $\alpha = 0.4$ with initial condition B as the initial condition.

for any width of the shear band region. It is to be noted that here $\alpha = 0$ excludes the liquid bridge distribution near the boundaries.

D. Dependence on the maximal liquid bridge volume

In this section we discuss the effect of increasing the maximal value on the overall dynamics of liquid redistribution. As a model simplification, we do not allow the formation of liquid clusters via bridge coalescence by using a maximal $V_{\max}$ of the bridge volumes which must not be exceeded. The maximal liquid bridge volume $V_{\max}$ is varied in different simulations as explained in Sec. II C, Eq. (5). Figure 10(a) shows the mean liquid bridge volume $\langle V_b \rangle$ as a function of local strain for different $V_{\max}$. Note that with an increase in $V_{\max}$ the maximum interaction distance between interacting particles i and j increases. Thus, the number of initial wet contacts increases with $V_{\max}$. The initial liquid bridge volume $V_b^0 \approx 11$ nl is kept the same for all the simulations. The peak liquid bridge volume V_p and the intermediate liquid bridge volume V_i also increase with increasing $V_{\max}$. Figure 10(b) shows that the number of wet contacts per particles decreases with increasing $V_{\max}$. Thus, allowing clustering of liquid leads to higher mean liquid bridge volume per contact and fewer wet contacts per particle in the intermediate pseudocritical state. However, for large enough β ($\beta > 0.1$), this limit parameter does not affect the system behavior anymore and the same steady state is reached irrespective of β. Thus, even for very large $V_{\max}$, the mean liquid bridge volume is well within the accuracy of the Willet *et al.* model, i.e., very few liquid bridges with large volumes are formed. This is significant, as it implies that it is not necessary to restrict the maximum allowed liquid bridge volume. Thus, even though $V_{\max}$ is very large for the extreme cases, $\langle V_b \rangle$ is well within the accuracy of the Willet *et al.* model, i.e., very few liquid bridges are formed which are of large liquid bridge volume. Thus, it is significant to note that we need not necessarily restrict the maximum allowed liquid bridge volume and can keep this as a free parameter.

E. Dependence on the liquid saturation

In this section we study the effect of liquid saturation on the liquid redistribution process. The bulk saturation is varied by varying the initial liquid film volume on the particles as mentioned in Sec. II D, Eq. (7). Figure 11(a) shows the mean

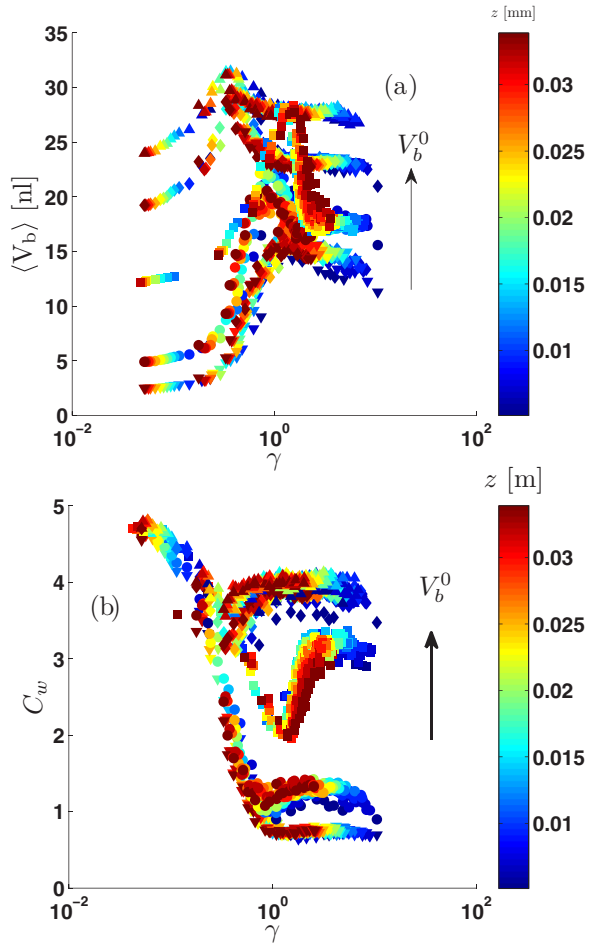

FIG. 11. (a) Mean liquid bridge volume per contact (b) number of wet contacts per particle as a function of local strain for different saturation $V_f^0 = 10$ nl (▽), $V_f^0 = 20$ nl (○), $V_f^0 = 50$ nl (□), $V_f^0 = 80$ nl (◇), and $V_f^0 = 100$ nl (△) for $\alpha = 0.4$ with initial condition B as the initial condition.

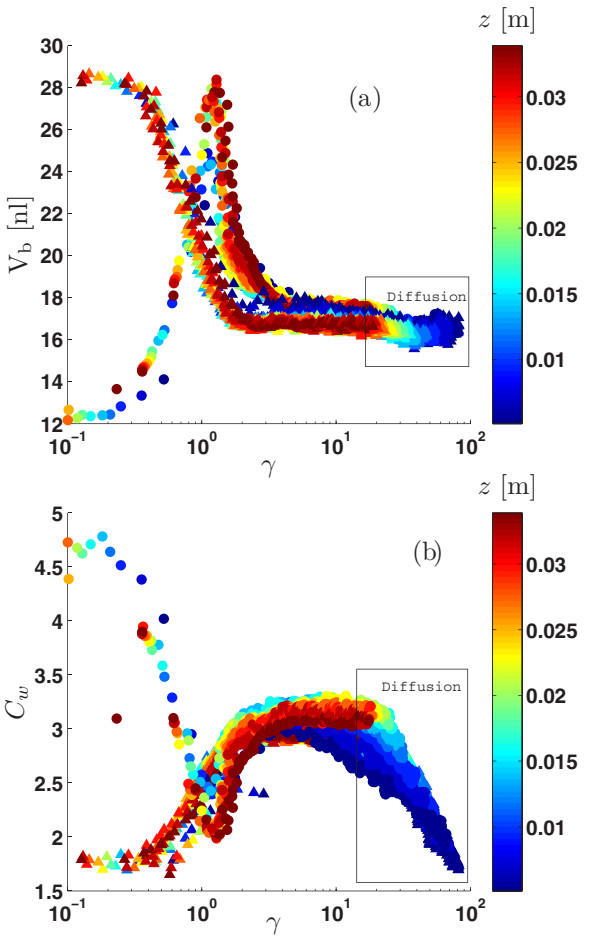

FIG. 12. (a) Mean liquid bridge volume per contact and (b) wet contacts per particle as a function of strain for initial condition A (△) and initial condition B (○).

liquid bridge volume for initial condition B as a function of local strain for different V_f^0. It is evident that the mean liquid bridge volume $\langle V_b \rangle$ increases with increasing saturation, i.e., bridges hold larger volumes of liquid with increasing saturation. All the other parameters, like the peak liquid bridge volume V_p and the intermediate state liquid bridge volume V_i, also increase with saturation. Figure 11(b) shows the mean fraction of wet contacts per particle for initial condition B as a function of local strain. The number of contacts per particle remains almost the same, which depends on the initial packing, irrespective of the local saturation. The number of wet contacts per particle increases with increasing saturation. Thus, both the mean liquid bridge volume per contact and the number of contacts per particle increase with increasing saturation in the system.

F. Diffusive and drift transport of liquid

There are two relevant processes that cause the spreading of liquid. First, it is known that in shear flows, particles undergo a self-diffusive motion and therefore liquid which is carried by the menisci will also diffuse in space [47,48]. The authors of those works observed that the particle or liquid diffusivity is proportional to the local shear rate in quasistatic dense flows. Second, there is a transport of liquid associated with liquid bridge rupture. The overall liquid migration is a non-steady-state diffusive process and occurs over a relatively larger scale of shear. The diffusive liquid transfer is triggered inside the shear band at the onset of shearing. However, the molecular diffusion mass transport mechanism is known to be a slower process. Hence, at the initial shear scale, the liquid redistribution dominates over the diffusive liquid transport process. This is shown in Figs. 12(a) and 12(b). The data shown in Fig. 8 are replotted in Fig. 12, but on a logarithmic scale and for a larger range of shear values, in order to show the long-shear-scale behavior of the liquid redistribution process.

Figure 12(a) shows the mean liquid bridge volume per wet contact inside the shear band as a function of local strain for initial conditions A and B. Figure 12(b) shows the fraction of wet contacts as a function of local strain inside the shear band for initial conditions A and B. A dramatic change in the mean liquid bridge volume and the number of wet contacts is observed during the initial phase of shearing. This is evidently the phase of liquid redistribution. The system reaches a pseudocritical state followed by this when both the

mean liquid bridge volume per contact and the number of wet contacts per particle reach a temporary steady state. On further shear, the mean volume of liquid bridge per contact decreases slightly and the number of wet contacts per particle slowly decreases. The overall liquid content decreases inside the shear band in the long term. This is evidently the regime when diffusive transfer of liquid is dominating. Though we state this mode of liquid transfer as a diffusive process, this liquid transfer equation is described as a drift-diffusive process in a different set of coordinate systems. These mechanisms of liquid transfer are interesting, but beyond the scope of the present study.

V. CONCLUSION

The transient behavior of liquid transport and redistribution are studied for different initial liquid distributions in a split-bottom ring-shear cell. This inhomogeneous system features a wide range of strain rates, the largest in the center of the shear band and practically in the tails, close to the walls. Therefore, given a certain time t, talking about (local) strain rate $\dot{\gamma}$ and talking about strain amplitude $\gamma = \dot{\gamma} t$ are equivalent. Governed by the rupture of existing and the formation of new liquid bridges, the initial distribution of liquid in the system reaches a pseudosteady or critical state within (local) shear strains of around $\gamma \lessapprox 2$–4, almost independent of the initial liquid distribution.

While rapid liquid redistribution is dominating at small shear strains, shear-driven slow liquid transport away from the shear band is dominating for larger shear strains above $\gamma \approx$ 10–20. The shear band becomes dry, devoid of wet contacts in the latter regime. Liquid is transported out (diffusionlike) towards the tails of the shear band.

Besides the initial conditions, the behavior at small strain rates is also influenced by the bulk saturation in the system and the liquid bridge limit volume imposed in our model. As expected, the mean liquid bridge volume per contact and the number of wet contacts per particle both increase with increasing saturation. Further, the mean liquid bridge volume per contact increases, but the number of wet contacts per particle decreases with increasing limit volume $V_{\max}$, ensuring conservation of liquid. For very large $V_{\max}$, the mean liquid volume probability distribution reaches a steady-state value with the majority of the contacts within the validity of the Willet *et al.* model and well below the volume needed to fill the pores; thus the liquid distribution is mostly unaffected by the limit parameter.

The first transient of liquid redistribution that is explained in this paper happens on a very short strain scale. During this phase, liquid is conserved within the shear band because it has no time to be transported away and only local rearrangement of the liquid bridges dominates, before a liquid front builds up and moves outward. The second transient happens at moderate to large strains and appears almost like a steady state due to the slowing down of the liquid front in the tails of the shear band. The third transient happens on an even larger strain (time) scale and leads to a complete drying of the shear band. We are now also theoretically studying the liquid transport on the large strain scale [49], under quasistatic conditions, when liquid is transported out of the shear band. While the simplest picture of diffusive transport with a constant diffusivity cannot explain the dynamics of liquid transport and the drying of the shear band, a model with a variable strain-rate-dependent coefficient of diffusion can [23]. However, the nonconstant diffusion leads to driftlike rather than diffusive features (rapid buildup and narrowing of the liquid front), making the basic understanding difficult. By transforming the variables, one can enforce a diffusion term with constant diffusivity, which yields a drift term with a variable drift coefficient. By decomposing the transport equations into drift and diffusion, the location of the peak liquid concentration can be predicted analytically, without having to numerically solving the transport equations. In the vicinity of the shear band center, where the Péclet number $\mathrm{Pe} \ll 1$, diffusion dominates drift. Away from the shear band center, where $\mathrm{Pe} \approx 1$, drift and diffusion become comparable.

Our present study on liquid bridge redistribution is limited to very small saturation of liquid in granular media. This works in the pendular regime where liquid bridges are present as distinct entities, connecting two particles. However, expecting this model to work beyond the pendular regime is questionable. Also, our results showing the evolution of liquid redistribution from different initial conditions need experimental validation, for completeness. The liquid bridge redistribution evolution is driven by the shear rate and is dependent on the local strain conditions. Thus, a generalization of our studies with varying shear rate is worth doing. Likewise, the model of liquid redistribution at breakup and forming of liquid bridges at contact relies on several simplifications that might not work for all materials and for faster shear rates and thus has to be tested experimentally.

ACKNOWLEDGMENTS

We acknowledge financial support through NWO-STW Project No. 12272, "Hydrodynamic theory of wet particle systems: Modeling, simulation and validation based on microscopic and macroscopic description."

[1] M. Gonzalez and A. M. Cuitiño, J. Mech. Phys. Solids **93**, 44 (2016).
[2] T. Müllner, K. K. Unger, and U. Tallarek, New J. Chem. **40**, 3993 (2016).
[3] A. J. Liu and S. R. Nagel, Nature (London) **396**, 21 (1998).
[4] Y. Jin and H. A. Makse, Physica A **389**, 5362 (2010).
[5] D. Bi, J. Zhang, B. Chakraborty, and R. P. Behringer, Nature (London) **480**, 355 (2011).
[6] F. Göncü, O. Durán, and S. Luding, C. R. Mec. **338**, 570 (2010).
[7] V. Ogarko and S. Luding, Soft Matter **9**, 9530 (2013).
[8] W. Lo, F. Yang, C. Chen, and S. Hsieh, Granular Matter **17**, 717 (2015).
[9] K. Kamrin and G. Koval, Comput. Part. Mech. **1**, 169 (2014).
[10] A. Jarray, V. Magnanimo, and S. Luding, Powder Technol. (2018), doi:10.1016/j.powtec.2018.02.045.

[11] D. L. Henann, J. J. Valenza, II, D. L. Johnson, and K. Kamrin, Phys. Rev. E **88**, 042205 (2013).
[12] N. Guo and J. Zhao, Comput. Geotech. **47**, 1 (2013).
[13] T. Kurtay and A. Reece, J. Terramech. **7**, 23 (1970).
[14] A. Sawicki and W. Świdziński, Arch. Hydro-Eng. Environ. Mech. **54**, 207 (2007).
[15] S. Roy, A. Singh, S. Luding, and T. Weinhart, Comput. Part. Mech. **3**, 449 (2016).
[16] S. Luding and F. Alonso-Marroquín, Granular Matter **13**, 109 (2011).
[17] A. Singh, V. Magnanimo, K. Saitoh, and S. Luding, New J. Phys. **17**, 043028 (2015).
[18] S. Roy, S. Luding, and T. Weinhart, New J. Phys. **19**, 043014 (2017).
[19] V. Richefeu, M. S. El Youssoufi, and F. Radjaï, Phys. Rev. E **73**, 051304 (2006).
[20] A. Ouazzi, *Finite Element Simulation of Nonlinear Fluids. Application to Granular Material and Powder* (Shaker, 2006)
[21] F. Radjai and V. Richefeu, Philos. Trans. A **367**, 5123 (2009).
[22] S. Roy, S. Luding, and T. Weinhart, EPJ Web Conf. **140**, 03065 (2017).
[23] R. Mani, D. Kadau, D. Or, and H. J. Herrmann, Phys. Rev. Lett. **109**, 248001 (2012).
[24] R. Mani, C. Semprebon, D. Kadau, H. J. Herrmann, M. Brinkmann, and S. Herminghaus, Phys. Rev. E **91**, 042204 (2015).
[25] R. Mani, D. Kadau, and H. J. Herrmann, Granular Matter **15**, 447 (2013).
[26] M. Scheel, R. Seemann, M. Brinkmann, M. Di Michiel, A. Sheppard, and S. Herminghaus, J. Phys.: Condens. Matter **20**, 494236 (2008).
[27] M. M. Kohonen, D. Geromichalos, M. Scheel, C. Schier, and S. Herminghaus, Physica A **339**, 7 (2004).
[28] S. Herminghaus, Adv. Phys. **54**, 221 (2005).
[29] F. Bianchi, M. Thielmann, R. Mani, D. Or, and H. J. Herrmann, Granular Matter **18**, 75 (2016).
[30] J. A. Dijksman and M. van Hecke, Soft Matter **6**, 2901 (2010).
[31] G. H. Wortel, J. A. Dijksman, and M. van Hecke, Phys. Rev. E **89**, 012202 (2014).
[32] A. Singh, V. Magnanimo, K. Saitoh, and S. Luding, Phys. Rev. E **90**, 022202 (2014).
[33] S. Luding, Part. Sci. Technol. **26**, 33 (2008).
[34] S. Luding, Particuology **6**, 501 (2008).
[35] R. Schwarze, A. Gladkyy, F. Uhlig, and S. Luding, Granular Matter **15**, 455 (2013).
[36] A. Gladkyy and R. Schwarze, Granular Matter **16**, 911 (2014).
[37] T. Weinhart, D. R. Tunuguntla, M. P. Van Schrojenstein Lantman, I. F. C. Denissen, C. R. Windows Yule, H. Polman, J. M. F. Tsang, B. Jin, L. Orefice, K. Van Der Vaart, S. Roy, H. Shi, A. Pagano, W. DenBreeijen, B. J. Scheper, A. Jarray, S. Luding, and A. R. Thornton, MercuryDPM: Fast, flexible particle simulations in complex geometries part II: Applications, in *5th International Conference on Particle-Based Methods - Fundamentals and Applications, PARTICLES, 2017* (International Center for Numerical Methods in Engineering, 2017), pp. 123–134.
[38] A. R. Thornton, D. Krijgsman, A. te Voortwis, V. Ogarko, S. Luding, R. Fransen, S. I. Gonzalez, O. Bokhove, O. Imole, and T. Weinhart, A review of recent work on the Discrete Particle Method at the University of Twente: An introduction to the open- source package MercuryDPM, in *Proceedings of DEM6-6th International Conference on Discrete Particle Method*, edited by G. Mustoe (Colorado School of Mines, Golden, CO, United States, 2013), pp. 50–56.
[39] C. D. Willett, M. J. Adams, S. A. Johnson, and J. Seville, Langmuir **16**, 9396 (2000).
[40] B. V. Derjaguin, Colloid Polym. Sci. **69**, 155 (1934).
[41] G. Lian, C. Thornton, and M. J. Adams, J. Colloid Interface Sci. **161**, 138 (1993).
[42] M. Scheel, R. Seemann, M. Brinkmann, M. Di Michiel, A. Sheppard, B. Breidenbach, and S. Herminghaus, Nat. Mater. **7**, 189 (2008).
[43] T. Weigert and S. Ripperger, Part. Part. Syst. Charact. **16**, 238 (1999).
[44] N. Mitarai and F. Nori, Adv. Phys. **55**, 1 (2006).
[45] A. Denoth, J. Glaciol. **28**, 357 (1982).
[46] A. Ries, D. E. Wolf, and T. Unger, Phys. Rev. E **76**, 051301 (2007).
[47] B. Utter and R. P. Behringer, Phys. Rev. E **69**, 031308 (2004).
[48] C. S. Campbell, J. Fluid Mech. **348**, 85 (1997).
[49] S. Roy, S. Luding, W. K. Otter, A. Thornton, and T. Weinhart (unpublished).